Performance Analysis of Altimeter-Aided GNSS Receiver for Indoor Scenarios

Fernando D. Nunes[(1)], Fernando M. G. Sousa[(2)], José M. N. Leitão[(3)]
[(1)]Instituto de Telecomunicações and IST
Av. Rovisco Pais, 1049-001, Lisboa, Portugal, email: nunes@lx.it.pt
[(2)]Instituto de Telecomunicações and ISEL
Rua Conselheiro Emídio Navarro, 1959-007, Lisboa, Portugal, email: fsousa@isel.pt
[(3)]Instituto de Telecomunicações and IST
Av. Rovisco Pais, 1049-001, Lisboa, Portugal, email: jleitao@lx.it.pt

***Abstract*—The paper addresses the problem of positioning inside buildings using a GNSS receiver. Since signals in indoor environments are very weak, a high-sensitivity receiver aided by a barometric altimeter is shown to be a suitable option. A specially tailored least-squares algorithm is proposed for the solution of the navigation equation. Simulation results prove that a well calibrated altimeter helps reduce significantly the positioning errors both in the vertical axis and in the horizontal plane.**

I. Introduction

In GNSS (Global Navigation Satellite Systems) the receiver position can be determined from a set of pseudorange measurements using, at least, $M = 4$ satellites in view. The achieved accuracy depends both on the pseudorange noise variance and on the geometry of the satellite sub-constellation in use. The "quality" of the geometry is often defined by the GDOP (geometric dilution of precision) parameter [1], [2], [3]. The GNSS available today (GPS, Glonass) or to be deployed in the near future (Galileo, Compass) are designed for outdoor applications where the signals are relatively strong (with typical carrier-to-noise ratios (C/N_0) around 45-50 dB-Hz). Recently, it was proposed to extend the usage of GNSS to indoor applications where the signals are in general much weaker due to the penetration through walls, ceilings, etc. [4]. For example, a typical concrete wall attenuates the GPS L1 signals (carrier frequency: 1.57542 GHz) around 10-15 dB [5].

Conventional receivers are unable to operate with $(C/N_0) < 20$ dB-Hz. In some cases, high sensitivity (HSGNSS) receivers can cope with those weak signals by increasing the integration intervals, provided that the platforms are fixed or slowly-moving, but the positioning accuracy is worse than the one achieved outdoors [4].

Using a non-coherent early-late processing (NELP) receiver with GPS C/A signals in the bandwidth-limited mode of operation, the pseudorange variance (expressed in square meters) due to thermal noise is given by [6]

$$\sigma_n^2 = c^2 T_c^2 \frac{B_n(1-0.5B_nT)}{2\left(\frac{C}{N_0}\right)} \frac{1}{BT_c}\left[1+\frac{1}{\left(\frac{C}{N_0}\right)T}\right] \quad (1)$$

where c is the speed of light, T_c is the chip duration, B_n is the noise equivalent bandwidth of the code tracking loop, T is the correlation (integration) interval, and B is the front-end bandwidth. Typical values for B_n and T are, respectively, 1 Hz and 0.01 s for outdoor applications [7]. Expression (1) is valid for $B_nT < 0.5$ and $B\Delta \leq 1$, with Δ denoting the delay lock-loop (DLL) early-late spacing. Reducing Δ permits to increase the front-end bandwidth B but the DLL tends to lose lock when $\Delta < 0.1T_c$ [3]. The receiver closed-loop bandwidth must be sufficiently wide to track the transient variation of delay versus time, which is caused by user-satellite range dynamics, without creating large transient errors [1]. This fact limits the minimum value that can be assigned to B_n for a given application.

In addition to thermal noise, pseudoranges are also affected by errors due to satellite clock and ephemeris parameters, atmospheric propagation modeling, multipath, etc. Typical variances for those disturbances are $\sigma_s^2 \approx 34\ \mathrm{m}^2$ [2]. Fig. 1 shows the rms tracking errors in meters for different noise bandwidths with $T = 0.01$ s and $BT_c = 5$ when the variances σ_n^2 and σ_s^2 are considered.

For indoor scenarios, with extra attenuations of 30 dB regarding outdoor reception (i.e., $(C/N_0) \leq 20$ dB-Hz), Fig. 1 shows that the pseudorange variances are highly dependent on the carrier-to-noise ratio (C/N_0) except for small values of B_n. Besides, whereas outdoor reception is characterized by small changes of carrier-to-noise ratio between satellites in view, in indoor scenarios the changes can be very significant as some signals may be received through a window (which introduces small attenuation) while the others have to penetrate the walls, thus being strongly attenuated.

II. Solving the equation of navigation

Let the known ECEF coordinates of satellite $i = 1, \ldots, M$ be given by $[x_i\ y_i\ z_i]^T$ and the receiver unknown coordinates be $[x_u\ y_u\ z_u]^T$. Alternatively, the receiver position can be defined by the geodetic parameters ϕ_u, λ_u and h_u, which are, respectively, latitude, longitude and altitude. The pseudoranges measured at the DLL output, after eliminating the offsets due to the extra propagation delays in the ionosphere/troposphere, are given by

$$\rho_i = \sqrt{(x_i-x_u)^2+(y_i-y_u)^2+(z_i-z_u)^2} - v_u + n_i \quad (2)$$

where $v_u = ct_u$ (t_u is the receiver clock offset) and $n_i \sim N(m_i, \sigma_i^2)$ are Gaussian r.v. that encompass the measurement errors such as satellite positioning errors, imperfect

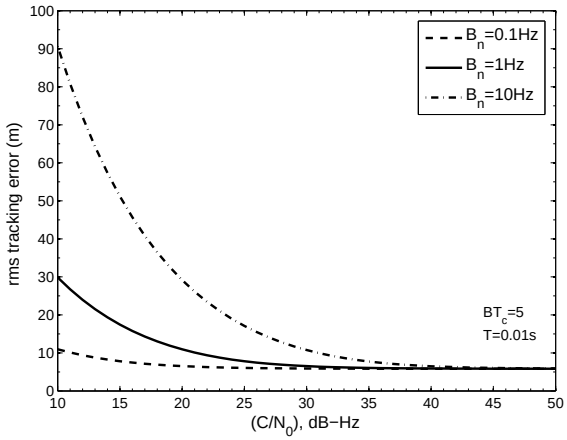

Fig. 1. Rms tracking errors for GPS C/A signals with different DLL noise equivalent bandwidths and a pseudorange variance of $\sigma_s^2 = 34$ m^2 due to other non thermal noise disturbances.

ionosphere and troposphere modeling, channel and receiver thermal noise, etc. The means m_i are usually considered to be zero except when there is multipath. The variances σ_i^2 depend on the values of σ_n^2 and σ_s^2 for each satellite.

A. without barometric altimeter

Consider that the following estimated vector $\widehat{X}_u = [\widehat{x}_u\ \widehat{y}_u\ \widehat{z}_u\ \widehat{v}_u]^T$ is currently available. The corresponding estimated pseudoranges are

$$\widehat{\rho}_i = \sqrt{(x_i - \widehat{x}_u)^2 + (y_i - \widehat{y}_u)^2 + (z_i - \widehat{z}_u)^2} - \widehat{v}_u. \quad (3)$$

Let $\Delta\rho_i \equiv \widehat{\rho}_i - \rho_i$. Assuming that $|\Delta\rho_i| \ll \rho_i$, the Taylor series development of the measured pseudoranges around $\widehat{\rho}_i$ (retaining only the linear terms) is

$$\rho_i = \widehat{\rho}_i + \frac{\partial\widehat{\rho}_i}{\partial\widehat{x}_u}\Delta x_u + \frac{\partial\widehat{\rho}_i}{\partial\widehat{y}_u}\Delta y_u + \frac{\partial\widehat{\rho}_i}{\partial\widehat{z}_u}\Delta z_u + \frac{\partial\widehat{\rho}_i}{\partial\widehat{v}_u}\Delta v_u \quad (4)$$

with

$$\begin{bmatrix} \frac{\partial\widehat{\rho}_i}{\partial\widehat{x}_u} \\ \frac{\partial\widehat{\rho}_i}{\partial\widehat{y}_u} \\ \frac{\partial\widehat{\rho}_i}{\partial\widehat{z}_u} \end{bmatrix} = -\frac{1}{\widehat{r}_i}\begin{bmatrix} x_i - \widehat{x}_u \\ y_i - \widehat{y}_u \\ z_i - \widehat{z}_u \end{bmatrix} \quad (5)$$

where

$$\widehat{r}_i = \sqrt{(x_i - \widehat{x}_u)^2 + (y_i - \widehat{y}_u)^2 + (z_i - \widehat{z}_u)^2} \quad (6)$$

and $\partial\widehat{\rho}_i/\partial\widehat{v}_u = -1$.

We obtain matricially

$$\begin{bmatrix} \Delta\rho_1 \\ \vdots \\ \Delta\rho_M \end{bmatrix} = \underbrace{\begin{bmatrix} -\frac{\partial\widehat{\rho}_1}{\partial\widehat{x}_u} & -\frac{\partial\widehat{\rho}_1}{\partial\widehat{y}_u} & -\frac{\partial\widehat{\rho}_1}{\partial\widehat{z}_u} & 1 \\ \vdots & \vdots & \vdots & \vdots \\ -\frac{\partial\widehat{\rho}_M}{\partial\widehat{x}_u} & -\frac{\partial\widehat{\rho}_M}{\partial\widehat{y}_u} & -\frac{\partial\widehat{\rho}_M}{\partial\widehat{z}_u} & 1 \end{bmatrix}}_{H} \begin{bmatrix} \Delta x_u \\ \Delta y_u \\ \Delta z_u \\ \Delta v_u \end{bmatrix}. \quad (7)$$

The least-squares solution for (7), with $M \geq 4$, is [3]

$$\begin{bmatrix} \Delta x_u \\ \Delta y_u \\ \Delta z_u \\ \Delta v_u \end{bmatrix} = (H^T H)^{-1} H^T \begin{bmatrix} \Delta\rho_1 \\ \vdots \\ \Delta\rho_M \end{bmatrix}. \quad (8)$$

Thus, at iteration k, the ECEF coordinates of the receiver's position are updated according to

$$\begin{bmatrix} \widehat{x}_u^{(k+1)} \\ \widehat{y}_u^{(k+1)} \\ \widehat{z}_u^{(k+1)} \\ \widehat{v}_u^{(k+1)} \end{bmatrix} = \begin{bmatrix} \widehat{x}_u^{(k)} \\ \widehat{y}_u^{(k)} \\ \widehat{z}_u^{(k)} \\ \widehat{v}_u^{(k)} \end{bmatrix} + \begin{bmatrix} \Delta x_u \\ \Delta y_u \\ \Delta z_u \\ \Delta v_u \end{bmatrix}. \quad (9)$$

B. with barometric altimeter

The iterative method in (9) requires, at least, $M = 4$ satellites in view, which is not always possible in urban canyons or, especially, in indoor environments. The introduction of a calibrated barometric altimeter permits to operate with only $M = 3$ satellites, thus increasing the percentage of time during which the equation of navigation can be solved.

The measurement of the barometric altimeter is well modeled as

$$\widehat{h}_u = h_u + n_h \quad (10)$$

where $\widehat{h}_u$ is the measured altitude and $n_h \sim N(m_h, \sigma_h^2)$ is a Gaussian r.v. For a calibrated altimeter $m_h = 0$. The relation between the pressure at an altitude $0 \leq h_u \leq 11$ Km and the sea level pressure P_0 is given by [8]

$$p = P_0\left(1 - 0.0065\frac{h_u}{T_0}\right)^{5.2561} \quad (11)$$

with $T_0 = 288.17$ K being the sea level standard absolute temperature. The altitude can be obtained from the atmospheric pressure measurement p according to

$$h_u = \frac{T_0}{0.0065}\left[1 - \left(\frac{p}{P_0}\right)^{0.1903}\right] \quad (12)$$

where $P_0 = 101325$ Pa is the sea level standard pressure. Besides the temperature and the altitude, the atmospheric pressure depends also on the weather conditions. That is why the barometric altimeter should be calibrated before use. However, due to possible weather changes, the calibration is useful only for a few hours. As an example, the Intersema MS5534C altimeter exhibits a rms error of ± 0.4 mbar, equivalent to $\sigma_h \approx 4$ meter at sea level [9]. Thus, to get a stable display it is necessary to take an average of minimum 4 consecutive pressure measurements.

The receiver Cartesian coordinates may be written in terms of the geodetic coordinates as [2]

$$\begin{bmatrix} x_u \\ y_u \end{bmatrix} = \left(\frac{a}{\sqrt{1 - e^2\sin^2\phi_u}} + h_u\right)\begin{bmatrix} \cos\lambda_u \\ \sin\lambda_u \end{bmatrix}\cos\phi_u \quad (13)$$

$$z_u = \left(\frac{a(1-e^2)}{\sqrt{1 - e^2\sin^2\phi_u}} + h_u\right)\sin\phi_u \quad (14)$$

where a is the length of the Earth semi-major axis and e is the eccentricity [2]. Consider the currently estimated geodetic parameters $[\widehat{\phi}_u\ \widehat{\lambda}_u\ \widehat{v}_u]^T$. Assuming that the altitude is perfectly known, the pseudoranges truncated Taylor's series around the currently estimated position are

$$\rho_i = \widehat{\rho}_i + \frac{\partial \widehat{\rho}_i}{\partial \widehat{\phi}_u}\Delta\phi_u + \frac{\partial \widehat{\rho}_i}{\partial \widehat{\lambda}_u}\Delta\lambda_u + \frac{\partial \widehat{\rho}_i}{\partial \widehat{v}_u}\Delta v_u. \quad (15)$$

But

$$\frac{\partial \widehat{\rho}_i}{\partial \widehat{\phi}_u} = \frac{\partial \widehat{\rho}_i}{\partial \widehat{x}_u}\frac{\partial \widehat{x}_u}{\partial \widehat{\phi}_u} + \frac{\partial \widehat{\rho}_i}{\partial \widehat{y}_u}\frac{\partial \widehat{y}_u}{\partial \widehat{\phi}_u} + \frac{\partial \widehat{\rho}_i}{\partial \widehat{z}_u}\frac{\partial \widehat{z}_u}{\partial \widehat{\phi}_u} \quad (16)$$

$$\frac{\partial \widehat{\rho}_i}{\partial \widehat{\lambda}_u} = \frac{\partial \widehat{\rho}_i}{\partial \widehat{x}_u}\frac{\partial \widehat{x}_u}{\partial \widehat{\lambda}_u} + \frac{\partial \widehat{\rho}_i}{\partial \widehat{y}_u}\frac{\partial \widehat{y}_u}{\partial \widehat{\lambda}_u} + \frac{\partial \widehat{\rho}_i}{\partial \widehat{z}_u}\frac{\partial \widehat{z}_u}{\partial \widehat{\lambda}_u} \quad (17)$$

with

$$\begin{bmatrix} \frac{\partial \widehat{x}_u}{\partial \widehat{\phi}_u} \\ \frac{\partial \widehat{y}_u}{\partial \widehat{\phi}_u} \end{bmatrix} = \left(\frac{a(1-e^2)}{(1-e^2\sin^2\widehat{\phi}_u)^{3/2}} - h_u \right) \sin\widehat{\phi}_u \begin{bmatrix} \cos\widehat{\lambda}_u \\ \sin\widehat{\lambda}_u \end{bmatrix} \quad (18)$$

$$\frac{\partial \widehat{z}_u}{\partial \widehat{\phi}_u} = \left(\frac{a(1-e^2)}{(1-e^2\sin^2\widehat{\phi}_u)^{3/2}} + h_u \right) \cos\widehat{\phi}_u \quad (19)$$

$$\begin{bmatrix} \frac{\partial \widehat{x}_u}{\partial \widehat{\lambda}_u} \\ \frac{\partial \widehat{y}_u}{\partial \widehat{\lambda}_u} \end{bmatrix} = \left(\frac{a}{(1-e^2\sin^2\widehat{\phi}_u)^{1/2}} + h_u \right) \cos\widehat{\phi}_u \begin{bmatrix} -\sin\widehat{\lambda}_u \\ \cos\widehat{\lambda}_u \end{bmatrix} \quad (20)$$

$$\frac{\partial \widehat{z}_u}{\partial \widehat{\lambda}_u} = 0. \quad (21)$$

From (15) we obtain $\Delta\rho_i \equiv \widehat{\rho}_i - \rho_i$, or matricially

$$\begin{bmatrix} \Delta\rho_1 \\ \vdots \\ \Delta\rho_M \end{bmatrix} = \underbrace{\begin{bmatrix} -\frac{\partial \widehat{\rho}_1}{\partial \widehat{\phi}_u} & -\frac{\partial \widehat{\rho}_1}{\partial \widehat{\lambda}_u} & 1 \\ \vdots & \vdots & \vdots \\ -\frac{\partial \widehat{\rho}_M}{\partial \widehat{\phi}_u} & -\frac{\partial \widehat{\rho}_M}{\partial \widehat{\lambda}_u} & 1 \end{bmatrix}}_{\widetilde{H}} \begin{bmatrix} \Delta\phi_u \\ \Delta\lambda_u \\ \Delta v_u \end{bmatrix}. \quad (22)$$

The least-squares solution for (22), with $M \geq 3$, is

$$\begin{bmatrix} \Delta\phi_u \\ \Delta\lambda_u \\ \Delta v_u \end{bmatrix} = (\widetilde{H}^T\widetilde{H})^{-1}\widetilde{H}^T \begin{bmatrix} \Delta\rho_1 \\ \Delta\rho_2 \\ \vdots \\ \Delta\rho_M \end{bmatrix}. \quad (23)$$

Thus, at iteration k, the geodetic parameters and the clock bias are updated according to

$$\begin{bmatrix} \widehat{\phi}_u^{(k+1)} \\ \widehat{\lambda}_u^{(k+1)} \\ \widehat{v}_u^{(k+1)} \end{bmatrix} = \begin{bmatrix} \widehat{\phi}_u^{(k)} \\ \widehat{\lambda}_u^{(k)} \\ \widehat{v}_u^{(k)} \end{bmatrix} + \begin{bmatrix} \Delta\phi_u \\ \Delta\lambda_u \\ \Delta v_u \end{bmatrix}. \quad (24)$$

Typically, 10 iterations are sufficient to guarantee the convergence of the algorithm. The estimated Cartesian coordinates are retrieved from (24) by resorting to (13)-(14) and assuming that the true altitude is the measured value $\widehat{h}_u$.

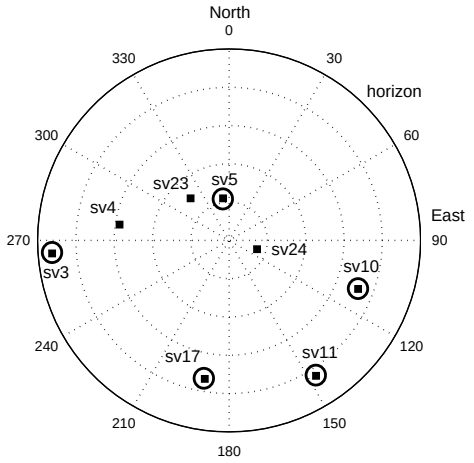

Fig. 2. Sky view of the visible satelites used in the simulations.

III. Simulation results

For outdoor scenarios, the best M satellites to be tracked depend on the sub-constellation geometry, i.e., the GDOP parameter, as the powers of the received signals are approximately equal, except for those very close to the horizon. A pre-defined mask angle is usually utilized to discard the satellites with very low elevation angles (typically lower than $5-7$ degrees) [3]. For indoor environments, the sub-constellation geometry is often less important than the attenuations and reflections suffered by the incoming signals as they penetrate the building. Signals received through windows usually experiment small additional attenuations (of about $2-3$ dB) whereas those received through a concrete wall or ceiling may present attenuations of about $10-20$ dB [5].

We consider the tracking of $M = 5$ GPS satellites (indicated by circles in Fig. 2) with a GDOP of 3.05. The position of the satellites was obtained in ECEF coordinates using the method presented in [10] with the parameters tabulated in [10], [11]. The receiver position is: $\phi_u = 39^{\circ}$ N, $\lambda_u = 9^{\circ}$ W and $h_u = 100$ m. The receiver parameters are: $BT_c = 5$, $T = 0.01$ s, and $B_n = 0.1$ Hz.

We simulate the determination of the receiver position with and without the aid of a barometric altimeter for a common indoor scenario. Fig. 3 shows the scatter plot of the horizontal error assuming a carrier-to-noise ratio $(C/N_0) = 20$ dB-Hz for the selected satellites without an altimeter. Figs. 4 and 5 exhibit the scatter plots obtained with $M = 3$ satellites (selected satellites: sv5, sv10, sv17) when a barometric altimeter is added. The barometric altimeter is assumed to have an error variance of $1\ \mathrm{m}^2$. Two cases are considered: in Fig. 4 the altimeter is calibrated, that is, the altitude estimation bias is zero; in Fig. 5 the altimeter is uncalibrated with a bias of $m_h = 10$ meters. Fig. 6 shows the altitude errors corresponding to the previously described scenarios. Note that the introduction of the altimeter reduces substantially the variance of those errors.

Comparing Figs. 4 and 5 it becomes clear the advantage

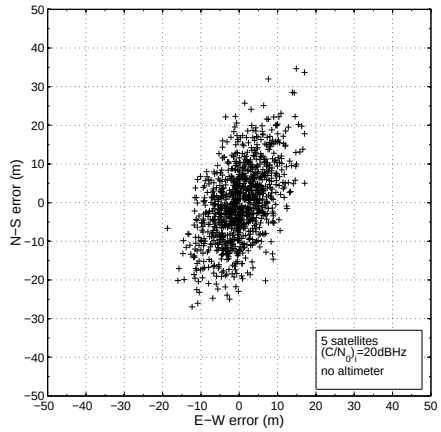

Fig. 3. Scatter plot of horizontal position error for 5 tracked satellites with $(C/N_0) = 20$ dB-Hz.

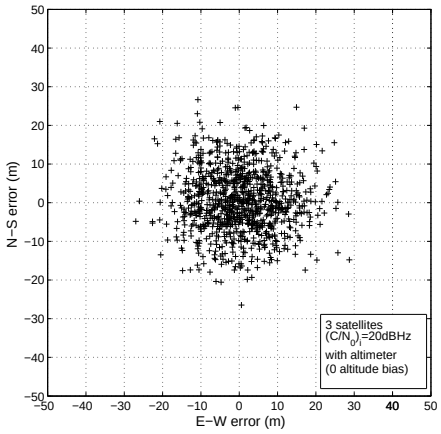

Fig. 4. Scatter plot of horizontal position error for 3 tracked satellites with $(C/N_0) = 20$ dB-Hz and a calibrated altimeter.

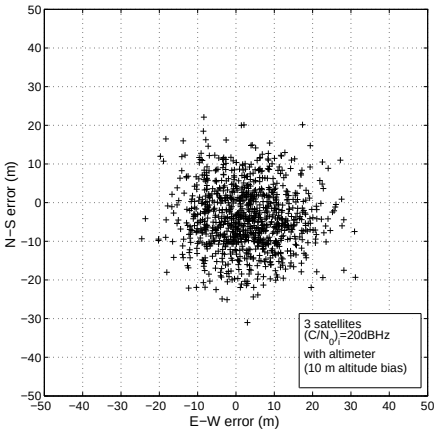

Fig. 5. Scatter plot of horizontal position error for 3 tracked satellites with $(C/N_0) = 20$ dB-Hz and an uncalibrated altimeter.

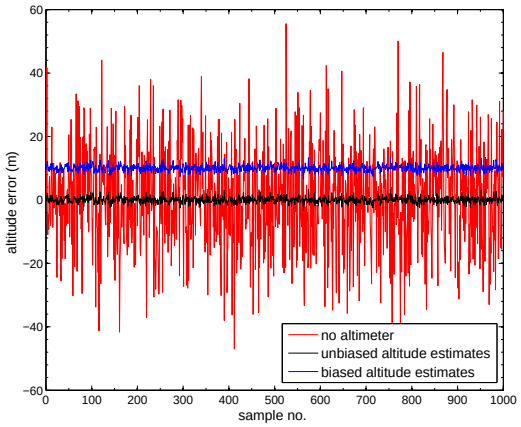

Fig. 6. Altitude errors obtained using (a) 5 satellites, (b) 3 satellites and a calibrated altimeter, and (c) 3 satellites and an uncalibrated altimeter. The standard deviation of the altitude error in (b) and (c) is equal to 1 meter.

of using a calibrated altimeter even for the position determination in the horizontal plane. In fact, whereas the spot in Fig. 4 is approximately centered at the correct position, the center of the spot in Fig. 5 is offset from the correct position by approximately $+2.7$ m in the E-W direction and -4.0 m in the N-S direction.

The results previously presented assume complete independence between samples (runs). In a practical situation, some filtering algorithm could be applied in order to minimize the variance of the position errors. A Kalman filtering approach requires the definition of models for the receiver's dynamics but is an efficient way to reduce those errors.

ACKNOWLEDGMENT

This work was motivated by the INPOS project, having as partners DEIMOS, INESC Inovação, and Instituto de Telecomunicações, which aims to develop a receiver for indoor positioning.

The paper was supported by the project PTDC/EEA-TEL/66918/2006 of the Portuguese Foundation for the Science and Technology (FCT).

REFERENCES

[1] B. Parkinson, J. Spilker, *Global Positioning System: Theory and Applications*, vol. I, AIAA, Washington DC, 1996.
[2] P. Misra, P. Enge, *GPS Positioning System, Signals, Measurements, and Performance*, Ganga-Jamuna, Lincoln, MS, 2004.
[3] E. Kaplan, C. Hegarty, *Understanding GPS. Principles and Applications*, second edition, Artech, Boston, 2006.
[4] G. Lachapelle et al., "HSGPS Signal Analysis and Performance under Various Indoor Conditions", *ION Navigation*, vol. 51, Spring 2004.
[5] W. Stone, "Electromagnetic Signal Attenuation in Construction Materials", NISTIR 6055, National Institute of Standards and Technology, 1997.
[6] J. Betz, K. Kolodziesjki, "Extended Theory of Early-Late Code Tracking for a Bandlimited GPS Receiver", *ION Navigation*, Vol. 47, no. 3, pp. 211-226, Fall 2000.
[7] K. Krumvieda et al., "A Complete IF Software GPS Receiver: A Tutorial about the Details", *ION GPS 2001*, Salt Lake City, UT, pp. 789-811, Sept. 2001.
[8] International Standard Atmosphere, ICAO document 7488/2.
[9] Intersema Application Note, AN501.
[10] R. Brown, P. Hwang, *Introduction to Random Signals and Applied Kalman Filtering*, third ed., Wiley, N. York, 1997.
[11] P. Massatt, F. Fritzen, "Assessment of the Proposed GPS 27-Satellite Constellation", *ION GPS/GNSS 2003*, pp. 399-406, Portland, OR, Sept. 2003.